ISSN 0023-1584, Kinetics and Catalysis, 2017, Vol. 58, No. 1, pp. 34–45. © Pleiades Publishing, Ltd., 2017.
Original Russian Text © N.I. Skripov, L.B. Belykh, T.P. Sterenchuk, V.V. Akimov, V.L. Tauson, F.K. Schmidt, 2017, published in Kinetika i Kataliz, 2017, Vol. 58, No. 1, pp. 36–48.

Factors Determining the Chemoselectivity of Phosphorus-Modified Palladium Catalysts in the Hydrogenation of Chloronitrobenzenes

N. I. Skripov[a], L. B. Belykh[a, *], T. P. Sterenchuk[a], V. V. Akimov[b], V. L. Tauson[b], and F. K. Schmidt[a]

[a] *Irkutsk State University, Irkutsk, 664003 Russia*

[b] *Vinogradov Institute of Geochemistry, Siberian Branch, Russian Academy of Sciences, Irkutsk, 664033 Russia*

**e-mail: belykh@chem.isu.ru*

Received May 18, 2016

Abstract—The precursor nature effect on the state of the Pd–P surface layer in palladium catalysts and on their properties in the liquid-phase hydrogenation of chloronitrobenzenes under mild conditions has been investigated. A general feature of the Pd–P-containing nanoparticles obtained from different precursors and white phosphorus at P/Pd = 0.3 ($PdCl_2$ precursor) and 0.7 ($Pd(acac)_2$ precursor) is that their surface contains palladium in phosphide form (BE(Pd3$d_{5/2}$) = 336.2 eV and BE(P2p) = 128.9 eV) and Pd(0) clusters (BE(Pd3$d_{5/2}$) = 335.7 eV). Factors having an effect on the chemoselectivity of the palladium catalysts in chloronitrobenzenes hydrogenation are considered, including the formation of small palladium clusters responsible for hydrogenation under mild conditions.

Keywords: hydrogenation, chloronitrobenzenes, palladium–phosphorus catalysts, chemoselectivity, X-ray photoelectron spectroscopy

DOI: 10.1134/S0023158417010104

The catalytic hydrogenation of chloronitrobenzenes is among the efficient chloroaniline synthesis methods that environmentally friendlier than the Bechamp reaction. The most common nitrohaloarene hydrogenation catalysts are group VIII metals (Pt, Pd, Ni, and Ru) [1, 2]. However, it is usually impossible to attain a high target product selectivity without using a modifier. A key problem in nitrohaloarene reduction with molecular hydrogen is to hamper the hydrogenolysis of the C–Hal bond, a process diminishing the haloaniline yield. The following approaches are traditionally used to prevent the hydrodehalogenation process: (1) modifying the metal catalysts with an S-, P-, or N-containing compound [2, 3], (2) varying the nature of the solvent [4–8] and support [9], (3) conducting the reaction via an electrochemical mechanism [10], (4) controlling the active component particle size [1, 2, 9], and (5) use of other, e.g., gold-containing catalysts [11–14].

In recent years, transition metal phosphides have been considered as new potential catalysts for hydrotreating processes (hydrodesulfurization [15–18] and hydrodenitrogenation [19, 20]). Although these phosphides are significantly less active than metal catalysts [21], they are more resistant to deactivation than metals and metal sulfides, carbides, and borides [19, 22], including in hydrodechlorination reactions [23]. At the same time, we demonstrated earlier [24, 25] that use of white phosphorus, a highly reactive phosphorus allotrope, as the phosphorus precursor of the catalyst makes it possible to obtain, under mild conditions (T = 80°C, P_{H_2} = 2 atm), Pd–P catalysts that are highly efficient in alkene and alkyne hydrogenation [24, 25] and are selective in the hydrogenation of *ortho*-chloronitrobenzene (*o*-CNB) [26]. The selectivity of the catalyst in *o*-CNB hydrogenation and the P/Pd ratio in the catalyst in the 0.3–1.0 range were observed to vary symbatically. Investigation of the nature of palladium catalysts obtained from $Pd(acac)_2$ and white phosphorus in a hydrogen atmosphere demonstrated that the high selectivity of the Pd–P catalysts (P/Pd = 0.3) in *o*-CNB hydrogenation is due to a thermodynamic factor, namely, an increase in the ratio of the *o*-CNB and *ortho*-chloroaniline (*o*-CA) adsorption equilibrium constants [26]. However, the reason why the selectivity of the catalyst increases with an increasing P/Pd ratio and the effect of the acido ligand in the precursor on the properties of the palladium catalysts still remain to be investigated.

For this purpose, we studied the palladium precursor effect on the state of the surface layer of the Pd–P catalysts at various P/Pd ratios and investigated their properties in the liquid-phase hydrogenation of chloronitrobenzenes.

EXPERIMENTAL

Materials

Solvents (benzene and *N,N*-dimethylformamide (DMF)) were purified using standard procedures [27]. Benzene was further dried by distillation from $LiAlH_4$ using a distillation column and was stored in an argon atmosphere in sealed tubes over molecular sieve 4A. For dehydration and amine removal, DMF was kept over anhydrous copper sulfate until the formation of a green solution and was then vacuum-distilled two times at a pressure of 8 Torr and a temperature no higher than 42°C.

Bis(acetylacetonato)palladium ($Pd(acac)_2$) was synthesized as described in Ref. [28] and was recrystallized from acetone. ^1H NMR (benzene): $\delta(CH)$ = 5.04 ppm (s, 1H), $\delta(CH_3)$ = 1.76 ppm (s, 6H). Palladium dichloride ($PdCl_2$, reagent grade) was used as received.

Dibenzylideneacetone (dba) was synthesized by reacting benzaldehyde with acetone [29]. Yellow, monoclinic, leaflike crystals of dba were dried on filter paper at room temperature in air and then under heating in a water bath in a vacuum (40°C/10 Torr) for 3 h.

Bis(dibenzylideneacetone)palladium(0) ($Pd(dba)_2$) was synthesized by reducing $PdCl_2$ with methanol in the presence of sodium acetate and dba [30]. Dibenzylideneacetone (3.4500 g, 1.472×10^{-2} mol), sodium acetate trihydrate (4.8525 g, 3.568×10^{-2} mol), and methanol (113 mL) were placed in a two-neck round-bottom flask. The reaction mixture was stirred at 50°C for 45–60 min to obtain a solution, and $PdCl_2$ (0.7875 g, 4.434×10^{-3} mol) was added. The resulting solution was stirred in an argon atmosphere at 40°C for 4 h. This yielded a dark violet precipitate of the $Pd(dba)_2$ complex, which was collected on a fritted glass filter under argon, washed with water and acetone, and vacuum-dried (30°C/2–3 Torr) for 3 h. The product yield was 2.4 g. (94% of the theoretical yield); T_m = 152°C. According to the literature, T_m of the $Pd(dba)_2$ complex is 152°C [31]. UV spectra: $Pd(dba)_2$, 525 nm ($d \rightarrow d^*$ transition, ε_{525} = 6400 L mol^{-1} cm^{-1}); non-coordinated dba, 325 nm ($n \rightarrow \pi^*$ transition, ε_{325} = 33540 L mol^{-1} cm^{-1}).

White phosphorus was mechanically cleaned to remove surface oxidation products and was washed with anhydrous benzene immediately before use. A solution of white phosphorus in benzene was prepared and stored in an inert atmosphere in a finger-shaped vessel that could be pumped and filled with argon. ^{31}P NMR: $\delta = -522$ ppm (s).

Ortho-, *meta*-, and *para*-chloronitrobenzenes were recrystallized from 95% ethanol and were then purified by distillation at a reduced pressure (*o*-CNB, 120°C/10 Torr; *m*-CNB, 111°C/10 Torr; *p*-CNB, 118°C/10 Torr).

Experimental Procedures

Chloronitrobenzene isomers were hydrogenated in a temperature-controlled, duck-shaped, glass shaker reactor at 30°C and an initial hydrogen pressure of 2 atm in the presence of a Pd–P catalyst formed in situ.

A solution of phosphorus in benzene (1 mL, 1.5×10^{-5}–3.5×10^{-5} mol of P) was added dropwise to a solution of $Pd(acac)_2$ (0.0152 g, 5×10^{-5} mol) in DMF (9 mL) in the temperature-controlled shaker reactor under flowing hydrogen, and the mixture was agitated for 5 min at room temperature. Next, the temperature was elevated to 80°C and the reaction mixture was agitated in a hydrogen atmosphere for 10–15 min. The resulting blackish brown "solution" was cooled to 30 or 50°C, and the substrate—*o*-, *m*-, or *p*-CNB was syringed into it. Hydrogenation was carried out under vigorous agitation to exclude diffusion limitations. Similar procedures differing only in temperature and catalyst formation time were used for other catalyst precursors. The catalytic systems based on $Pd(dba)_2$ and $PdCl_2$ were prepared at 30°C for 10 min.

Chloronitrobenzene hydrogenation was monitored by measuring the pressure drop in the system with a manometer and by analyzing the reaction mixture by gas–liquid chromatography on a Khromatek-Kristall 5000 chromatograph (Chromatec, Russia) fitted with a 30-m-long capillary column (BPX-5 phase, 5% diphenyl–95% dimethyl polysilphenylene siloxane) and a flame-ionization detector. Analyses were performed in a temperature-programmed mode (180°C, 5 min; 270°C, 15 min; heating rate, 30 deg/min). Intermediates and reaction products were additionally identified using a GCMS-QP2010 Ultra gas chromatograph–mass spectrometer system (Shimadzu, Japan) with a GsBP·5MS capillary column (30 m, BPX-5 phase). Electron-impact ionization with an electron energy of 70 eV was used. The *o*-CA selectivity was calculated via the formula

$$S_{o\text{-CA}} = \frac{C_{o\text{-CA}}}{C^0_{o\text{-CNB}} - C_{o\text{-CNB}}} \times 100,$$

where $C_{o\text{-CA}}$ is the current *o*-CA concentration and $C^0_{o\text{-CNB}}$ and $C_{o\text{-CNB}}$ are the initial and current *o*-CNB concentrations, respectively.

Methods of Characterization of Pd–P Catalysts

Micrographs of catalyst samples were obtained by high-resolution transmission electron microscopy (HRTEM) and Z-contrast scanning transmission electron microscopy (STEM) using a Tecnai G^2 microscope (FEI, United States) at an accelerating voltage of 200 kV. Colloidal solutions of Pd–P catalysts were diluted with DMF by a factor of 5. A drop of the resulting solution was placed on a carbon-coated copper grid (200 mesh) and was dried at room tem-

Table 1. Palladium precursor effect on the activity and selectivity of Pd–P catalysts in *o*-CNB hydrogenation

Precursor	P/Pd	Reaction time, min	Conversion, %	Product yield, mol %			Initial turnover frequency, $mol_{H_2} mol^{-1}_{Pd\Sigma}\ min^{-1}$
				o-CA	aniline	others[a]	
$Pd(acac)_2$	0	6	54	38.3	4.9	56.8	20.0
		570	99	50.4	17.1	32.5	
		24 h	100[b]	56.9	19.0	24.1	
	0.3	30	73	41.8	6.6	51.6	4.0
		122	99	65.6	11.6	22.8	
		246	100[b]	73.1	14.6	12.4	
	0.7	30	54	47.2	1.8	51.0	2.7
		96	99	64.3	3.5	32.2	
		325	100[b]	90.6	9.0	0.4	
$PdCl_2$	0	209	56	44.6	12.0	43.4	4.0
		684	97	45.7	18.8	35.5	
	0.3	185	72.3	48.2	3.4	48.4	2.7
		288	99	87.5	7.0	5.5	
$Pd(dba)_2$[c]	0	146	52	48.0	16.7	35.3	34.5
		230	57	45.5	15.6	38.9	
	0.3	48	55	29.8	6.7	63.5	18.1
		180	99	54.9	11.4	33.7	

Reaction conditions: C_{Pd} = 5 mmol/L, *o*-CNB/Pd = 87, T = 30°C, P_{H_2} = 2 atm, solvent—10 mL of DMF.

[a] *o*-Chlorophenylhydroxylamine, 2,2'-dichloroazoxybenzene, 2,2'-dichloroazobenzene, 2-chlorobenzene (traces), and 4-(2-chlorophenyl)iminopentan-2-one.

[b] Further hydrogenation after complete *o*-CNB conversion.

[c] $Pd(dba)_2$ concentration of 1 mmol/L.

perature in an inert atmosphere in a glovebox. Images were recorded with a CCD camera (Soft Imaging System, Germany). The device was equipped with an energy-dispersive X-ray spectrometer (EDX, Phoenix) with a Si(Li) semiconductor detector. Particle image parameters in the micrographs were measured using the iTEM 5.0 and DigitalMicrographs 1.94.1613 programs. An analysis of periodic structures and image filtering, were carried out by the fast Fourier transformation (FFT) and inverse fast Fourier transformation (IFFT) methods. For constructing particle size histograms, we selected areas containing at least 300–350 particles.

X-ray photoelectron spectra (XPS) were recorded on a PHOIBOS 150 MCD 9 spectrometer (SPECS, Germany) using monochromatic AlK_α radiation from an X-ray tube (1486.74 eV). A survey spectrum was recorded using 1 eV steps at an analyzer pass energy of 30 eV; high-resolution spectra (narrow scans), using 0.05 eV steps at a pass energy of 10 eV. The C1*s* line (285.0 eV) was taken to be the binding energy reference. The nonuniform charging effect was eliminated by irradiating the sample by slow electrons. Samples were sputtered with Ar^+ ions for 1 min using a PU-IQE112/38 scanning ion gun (SPECS) at an accelerating voltage of 2.5 kV and an ion current of 20 μA, which ensured a sputtering rate of ~0.5 nm/min. Experimental data were processed using the CasaXPS program. The spin–orbit split doublet lines Pd3$d_{5/2-3/2}$ and P2$p_{3/2-1/2}$ were approximated by two Lorentzian–Gaussian curves with interdoublet spacings of 5.26 and 0.84 eV, respectively, at a fixed peak area ratio of 3/2 for Pd3$d_{5/2-3/2}$ and 2/1 for P2$p_{3/2-1/2}$. The full width of spectral lines at (FWHM) was refined in an interval of up to 1.5 eV (1.0 eV for phosphorus). It was assumed that, if FWHM > 1.5 eV (>1.0 eV for phosphorus), then the line should be approximated by several curves corresponding to chemical species of the element. Because the oxygen 1*s* line is heavily overlapped with the palladium 3$p_{3/2}$ line, the number of palladium species and the positions of the corresponding lines were harmonized with the second doublet in the survey spectrum—Pd3$p_{1/2}$.

RESULTS AND DISCUSSION

In order to elucidate the precursor effect on the properties of the Pd–P catalysts in *o*-CNB hydrogenation, we studied the systems based on $Pd(acac)_2$, $PdCl_2$, and the palladium(0) complex $Pd(dba)_2$. Table 1

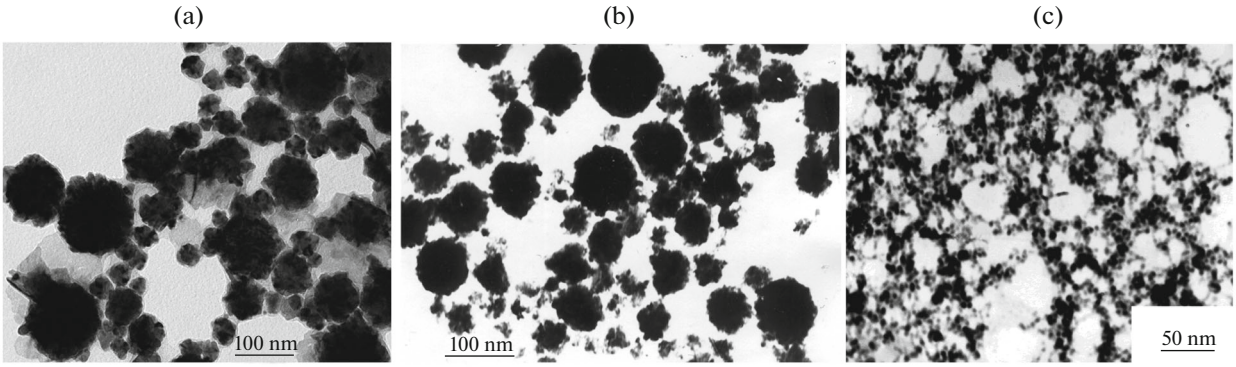

Fig. 1. TEM images of the blacks obtained from (a) $Pd(acac)_2$, (b) $PdCl_2$, and (c) the Pd(0) complex–$Pd(dba)_2$ in DMF in a hydrogen atmosphere.

presents the results of our investigation of the properties of Pd blacks and Pd–P catalysts prepared from different palladium compounds in a hydrogen atmosphere in a DMF medium in the presence of white phosphorus.

The palladium blacks forming from $Pd(acac)_2$, $PdCl_2$, and $Pd(dba)_2$ in a hydrogen atmosphere in the absence of white phosphorus differ in their catalytic activity and *o*-CA selectivity. The blacks obtained from $Pd(dba)_2$ or $Pd(acac)_2$ show a high initial activity, but, because of their rapid aggregation leading to the formation of a precipitate, the turnover frequency of the catalyst decreases dramatically (by more than one order of magnitude) after 50% *o*-CNB conversion is reached. As a consequence, in spite of the long duration of the process, it is impossible to hydrogenate the entire *o*-CNB and the forming intermediates (Table 1). The variation of turnover frequency from one Pd black to another is possibly associated with their degree of dispersion, since their base particle size depends both on the nature of the precursor and on their initial concentration (Fig. 1). The particle diameter of the Pd black forming from $Pd(acac)_2$ at an initial concentration of 5 mmol/L ranges between 21 and 122 nm. The average particle diameter is 48 nm (Fig. 1a). Since, according to TEM data, the size of some Pd black particles is larger than the crystallite size determined by X-ray diffraction (20 nm), these large particles are aggregates. A similar situation was observed for the black obtained from $PdCl_2$ (Fig. 1b). As is clear from the TEM image of this black, the aggregates, whose average size is 37 nm, consist of base particles ~7 nm in diameter. The smallest particle size is observed for the black obtained from $Pd(dba)_2$ ($d \approx 3$ nm, Fig. 1c).

As follows from the data presented in Table 1, the black forming from $PdCl_2$ is less active than the black obtained from $Pd(acac)_2$, although the average aggregate sizes in these two blacks are similar (Fig. 1). Therefore, the particle size of the blacks is not the only factor in their catalytic activity. In the hydrogenolysis of $Pd(acac)_2$, acetylacetone forms in the reaction mixture, while $PdCl_2$ reduction yields HCl, a strong acid. The poisoning effect of chloride ions on the Pd–P hydrogenation catalysts was earlier demonstrated for ammonium chloride as an example [25]. The introduction of NH_4Cl ($NH_4Cl/Pd = 1$) diminished, by a factor of 2, the activity of the catalyst formed from $Pd(acac)_2$ ($P/Pd = 0.3$) in styrene hydrogenation, a model reaction. Here, not only the resulting HCl can be the catalyst poison. It was found experimentally that hydrochloric acid accelerates the hydrolysis of the solvent (DMF) by water traces present in the latter, which results in the formation of dimethylammonium chloride [25]. This compound adsorbs onto the Pd black surface and acts as a catalyst poison reducing the turnover frequency of the catalyst and as a stabilizer enhancing the stability of the nanosystem.

The nature of the palladium precursor has an effect not only on the activity of the Pd blacks but also on the *o*-CA selectivity. Although the *o*-CA selectivity is not high for all of the Pd blacks (which is a general feature of palladium catalysts), it is necessary to consider the composition of the *o*-CNB conversion products. The selectivity is decreased by the hydrogenolysis of the C–Cl bond and by the condensation of intermediates (*ortho*-chlorophenylhydroxylamine and nitrosochlorobenzene) in DMF, a weakly basic solvent. At ~50% *o*-CNB conversion, the degree of hydrogenolysis of the C–Cl bond in the presence of the black obtained from $Pd(acac)_2$ is almost 3 times lower than in the presence of the black derived from $Pd(dba)_2$ (Table 1). Since the formation of these blacks is not accompanied by the formation of a catalyst poison, they are convenient objects for analyzing the particle size effect on selectivity. The fact that the degree of hydrogenolysis decreases with an increasing size of base Pd black particles is consistent with the view that this reaction is size-sensitive because *o*-CNB adsorption on large palladium particles is preferential compared to *o*-CA adsorption [32]. The hydrogenolysis of the C–Cl bond in chloroanilines over heterogeneous Pt catalysts

Table 2. Hydrogenation of *m*- and *p*-CNB in the presence of the $Pd(acac)_2$–*n*P catalytic system

Substrate	*T*, °C	P/Pd	Reaction time, min	CNB conversion, %	Product yield, mol %		
					CA	aniline	others*
p-CNB	30	0.3	215	100	73.7	1.6	24.7
	30	0.7	180	100	78.4	5.7	15.9
	50	0.7	90	100	77.2	13.1	9.7
m-CNB	50	0.3	80	100	68.6	10.9	20.5
	50	0.7	105	100	81.4	9.4	9.2

Reaction conditions: C_{Pd} = 5 mmol/L, substrate/Pd = 87, P_{H_2} = 2 atm, solvent—10 mL of DMF.

* 3,3'-Dichloroazoxybenzene and 3,3'-dichloroazobenzene (or 4,4'-dichloroazoxybenzene and 4,4'-dichloroazobenzene) and 4-(2-chlorophenyl)iminopentan-2-one.

proceeds more readily when the diameter of the platinum nanoclusters is 3–5 nm [1, 2].

The introduction of phosphorus before catalyst formation exerts a promoting effect on the chemoselectivity of the Pd–P-containing particles. The *o*-CA selectivity increases with an increasing P/Pd ratio (Table 1). The properties of the Pd–P catalysts obtained from $Pd(acac)_2$ and $PdCl_2$ at P/Pd = 0.3 differ, while the turnover frequencies of the catalysts obtained at P/Pd = 0.3 and 0.7 and their *o*-CA selectivities are similar (Table 1). The effect of the nature of the acido ligand in the precursor on the optimum P/Pd ratio at which a high *o*-CNB hydrogenation selectivity is achieved may arise from the difference between the rates at which $Pd(acac)_2$ and $PdCl_2$ are reduced by phosphorus and hydrogen and, as a consequence, the formation of different reduced species. $Pd(acac)_2$, which contains O,O-chelating acac ligands, is reduced by phosphorus at a three times lower rate than $PdCl_2$ [25]. In addition, as compared to the reduction of palladium dichloride by hydrogen, the reduction of $Pd(acac)_2$ takes places under severer conditions (80°C).

The promoting effect of phosphorus on the palladium catalysts was also observed in the hydrogenation of other isomers, namely, *m*- and *p*-CNB. The main regularities in the hydrogenation of *p*-CNB and *m*-CNB in the presence of the Pd–P catalysts are the same as in *o*-CNB hydrogenation: in the reduction of these isomers, the selectivity again increases with an increasing P/Pd ratio owing to the decreasing extent of C–Cl bond hydrogenolysis or condensation product formation. With an increasing temperature, the contribution from hydrogenolysis to the overall process increases (Table 2). Irrespective of the temperature, during the reduction of *m*- and *p*-CNB the reaction medium contains no chlorophenylhydroxylamine, an undesired intermediate, and the selectivity of the Pd–P catalyst toward the formation of *m*- and *p*-CA, respectively, remains practically invariable (60–73%).

The decrease of *o*-CNB hydrogenation activity on passing from Pd black to the Pd–P catalysts may be due to the decrease in the number of active sites or to a change in their nature and, accordingly, in their reactivity; it can be a result of the action of a catalyst poison as well. In turn, the increase in selectivity indicates a change in the nature of active sites or the appearance of an inhibitor whose displacement from an active site depends on the adsorbability of the substrate. In order to experimentally elucidate the cause of the modifying action of phosphorus, we considered the nature and state of the surface layer of the Pd–P catalysts.

According to TEM data, the reduction of $PdCl_2$ with hydrogen (P/Pd = 0.3, sample 1) yields a fine-particle (Fig. 2). The average particle size in this system (2.7 ± 0.86 nm) is comparable with the crystallite size calculated via the Selyakov–Scherrer formula from X-ray diffraction (XRD) data (3.4 nm). The HRTEM images of different areas of the $PdCl_2$–$0.3P$–H_2 system show interplanar spacings of 2.41, 2.38, 2.26, 2.226, and 2.116 Å, which correspond the phosphide Pd_9P_2 (*d*/*n* (hkl) = 2.414 (–113), 2.385 (122), 2.26 (130), 2.225 (211) and 2.116 (–123) Å; # 00-019-0890). The interplanar spacings 2.26, 2.103, and 1.455 Å pertain to the phosphide Pd_6P (*d*/*n* = 2.255 (030), 2.107 (130) and 1.456 (–153) Å; # 00-029-0966). One of the HRTEM images is presented in Fig. 2. The HRTEM data suggest that palladium phosphide Pd_9P_2 and/or Pd_6P forms in the $PdCl_2$–$0.3P$–H_2 system under mild conditions. Because of the small particle size in sample 1, the XRD characterization of this sample did not ultimately clarify this issue, since the strongest reflections from palladium metal and the palladium phosphides occur in the $2\theta = 40°$ region.

According to potentiometric titration data, at P/Pd = 0.3 phosphorus reduces ~34% of the $PdCl_2$ [25]. The remaining 66% of the palladium dichloride is reduced by hydrogen. The stoichiometry of the process suggests that 0.22 mol of P_4 (in terms of the atomic form of P_4) is spent on $PdCl_2$ reduction by phosphorus and 0.08 mol of the 0.3 mol of phosphorus is spent on the formation of the palladium phosphides:

$$3PdCl_2 + 2P + 6H_2O = 3Pd(0) + 6HCl + 2H_3PO_3,$$

$$xPd(0) + ¼P_4 = Pd_xP.$$

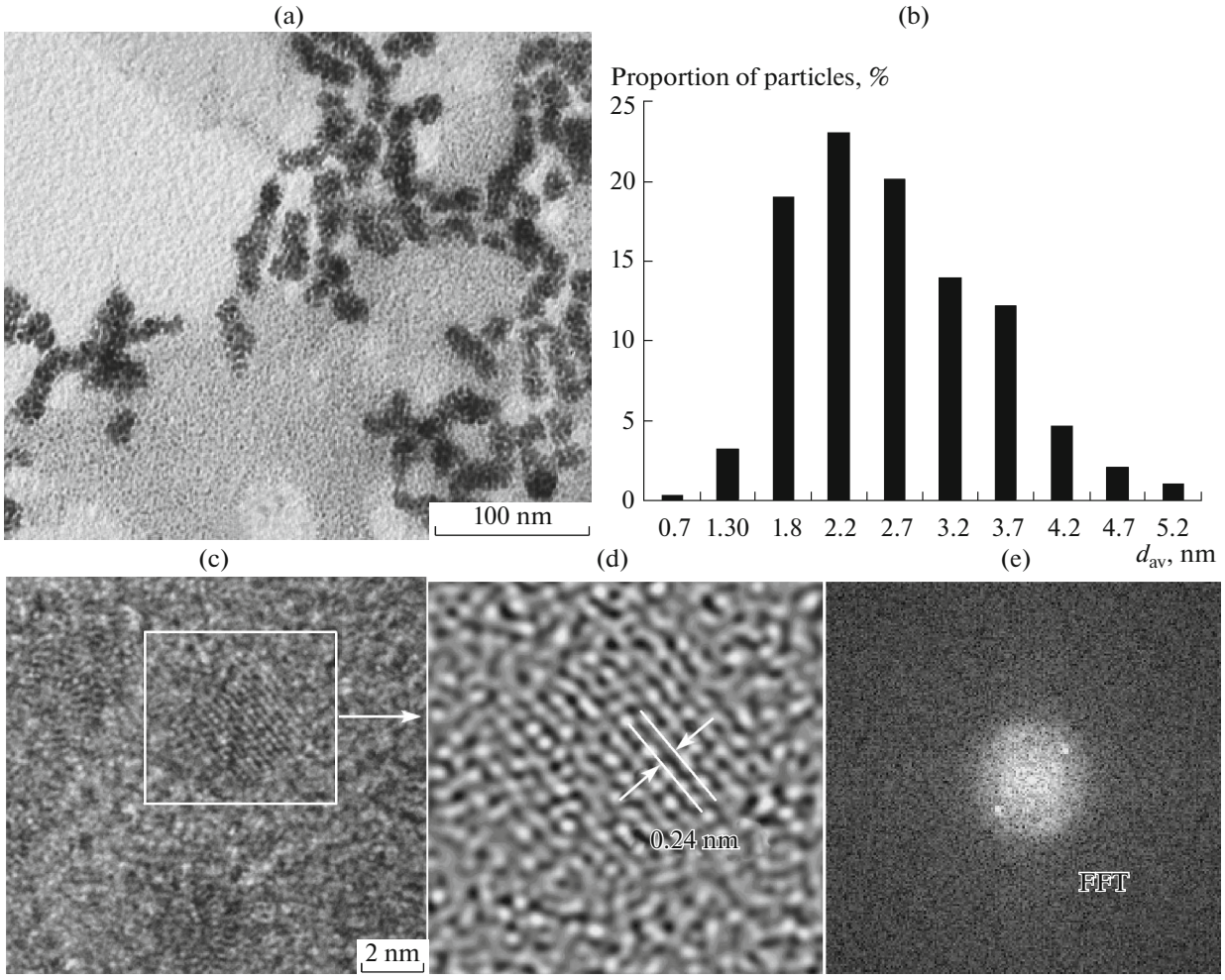

Fig. 2. (a) TEM image of the $PdCl_2$–0.3P–H_2 system formed in DMF, (b) particle size distribution, (c, d) HRTEM images of the system, and (e) FFT pattern.

Since the entire palladium dichloride in the $PdCl_2$–0.3P–H_2 system undergoes conversion, the palladium-to-phosphorus ratio must correspond to the formula $Pd_{12.5}P_1$. This Pd content is higher than that of $Pd_{15}P_2$, the palladium phosphide richest in palladium [33]. Therefore, the sample contains palladium and a mixture of its phosphides. The formation of Pd(0) is consistent with XPS data.

According to XPS data, palladium on the surface of the Pd–P catalyst prepared from $PdCl_2$ and white phosphorus in a hydrogen atmosphere (P/Pd = 0.3) is in three chemical forms characterized by Pd3$d_{5/2}$ electron binding energies of 335.7, 336.2, and 337.2 eV (Table 3, Fig. 3a). All of these three values exceed the binding energy for palladium metal (BE(Pd3$d_{5/2}$) = 335.2 eV), indicating that these palladium species bear a partial positive charge ($Pd^{\delta+}$). The ratio of the surface atomic concentrations of these species is 33 : 41 : 25. The Pd3$d_{5/2}$ binding energy value 336.2 eV characterizes the state of palladium in the palladium phosphides (BE (Pd3$d_{5/2}$) = 336.2 eV) [34]. This assumption is consistent with the presence of a BE = 129.8 eV peak in the P2*p* spectrum. In metal phosphides, BE(P2*p*) depends only slightly on the nature of the transition metal and typically varies between 128.5 and 130 eV [35].

It is more difficult to interpret the Pd3$d_{5/2}$ spectral component observed at BE = 335.7 eV. The positive shift of this energy can be due to both the formation of a surface (2D) palladium oxide [36] and the formation of small palladium clusters ($d \approx 1$ nm) [37, 38]. The surface layers of Pd_5O_4 2D oxide are characterized by XPS peaks at BE(Pd3$d_{5/2}$) = 335.5 eV and BE(O1*s*) = 528.9 eV [36]. The absence of an O1*s* peak at 528.9 eV rules out the formation of a 2D palladium oxide (Table 3). For this reason, the Pd3$d_{5/2}$ spectral component at 335.7 eV was assigned to small palladium clusters, for which this energy is ~336 eV. In particular, the binding energy of the Pd3$d_{5/2}$ component changes from 336.9 eV for Pd_1 to 336.1 eV for Pd_{10} [39]. The surface atomic concentrations of palladium as clusters

Table 3. Binding energies and concentrations of elements in different states in the surface layer of the Pd–P catalyst prepared from $PdCl_2$ and P_4 in a hydrogen atmosphere (P/Pd = 0.3)

Spectral line	Binding energy, eV	FWHM, eV	Element concentration, at %	Most likely chemical species*
Pd3$d_{5/2}$	335.7	1.0	13.9	Pd^0 (0.33)
	336.2	1.3		Pd_xP (0.41)
	337.2	1.5		Pd–Cl (0.26)
P2$p_{3/2}$	129.8	0.8	13.0	Pd_xP (0.37)
	130.9	1.0		P (0.15)
	132.6	1.0		HPO_3^{2-} (0.22)
	133.5	1.0		HPO_4^{2-} (0.09)
	134.1	1.0		$H_2PO_4^-$ (0.17)
N1s	402.1	1.5	2.1	$[NH_2R_2]^+$ (1.0)
O1s	531.4	1.5	15.2	HPO_3^{2-}, $H_2PO_4^-$ (1.0)
C1s	284.3	0.9	50.7	Pd_xC, graphite (0.14)
	285.0	1.5		C–H, C–C (0.52)
	286.2	1.5		$[NH_2R_2]_2X$ (C–N) (0.25)
	288.9	1.5		acacH (C=O) (0.06)
	292.4	0.8		CO_2, CO_3 (0.03)
Cl2$p_{3/2}$	198.1	1.1	5.1	Pd–Cl (1.0)

* The number in parentheses is the atomic fraction of the species.

and phosphides are similar: Pd(0) : Pd_xP = 1 : 0.8 (Table 3).

The surface of the Pd–P catalyst contains chlorine for which the Cl2$p_{3/2}$ binding energy corresponds to the chloride ion Cl^- (BE(Cl2$p_{3/2}$) = 198.2 eV [40]). For the covalently bonded or nonionized chlorine atom Cl^0, BE(Cl2$p_{3/2}$) = 200.3 eV [41]. Since Pd3$d_{5/2}$ electron binding energy for $PdCl_2$ is 337.5 eV [42], the third chemical form of palladium is assignable to PdCl surface fragments [43]. The atomic surface concentrations of Pd (BE(Pd3$d_{5/2}$) = 337.2 eV) and Cl are close to one another (Pd : Cl = 3.5 : 5).

Note that phosphorus on the surface of the Pd–P catalyst (P/Pd = 0.3, $PdCl_2$ precursor) is both in the form of phosphides (BE(P2$p_{3/2}$) = 129.8 eV) [36] and in oxidized forms, namely, hydrophosphites (132.6 eV) [44], hydrophosphates (133.5 eV) [20], and dihydrophosphates (134.1 eV) [20] (Table 3). The composition of the surface phosphides, which is representable by the empirical formula $Pd_{1.2}P$, indicates that the nanoparticles surface is enriched with phosphorus. In addition, the P2p photoelectron spectra contain a peak at a binding energy of 130.9 eV. A similar P2p peak (BE = 131.1 eV) was observed by other authors [45] for nanoparticles obtained from palladium dichloride and white phosphorus in an ethanolic medium but at higher temperature and larger P/Pd ratios (80°C, P/$PdCl_2$ = 1.5). The absolute P2p binding energy value 130.9 eV corresponds to elemental phosphorus. This suggests that the catalyst surface contains coordinated adsorbed phosphorus; however, it is still impossible to better substantiate the assignment of this spectral component.

The accumulation of phosphorus on the particle surface suggests the following hypothesis concerning the mechanism of the formation of the Pd–P catalyst from $PdCl_2$ and white phosphorus in a hydrogen atmosphere at P/Pd = 0.3. The formation of a highly dispersed system in this case indicates that the nucleation rate is higher than the particle growth rate. A distinctive feature of the Pd–P catalyst is that it contains small palladium clusters. Since even white phosphorus, a very reactive form of phosphorus, does not react with palladium nanoclusters below 180°C [46], it can be hypothesized that, because of the high rate of $PdCl_2$ reduction by phosphorus and hydrogen, part of the resulting Pd(0) atoms reacts with P_4 to yield Pd_9P_2 and Pd_6P and the other part turns into palladium clusters that do not react with P_4 under mild conditions. It is commonly accepted that the high-temperature synthesis of metal phosphides (250–700°C) from various phosphorus precursors (PO_4^{3-}, PO_3^{3-}, PH_3) proceeds

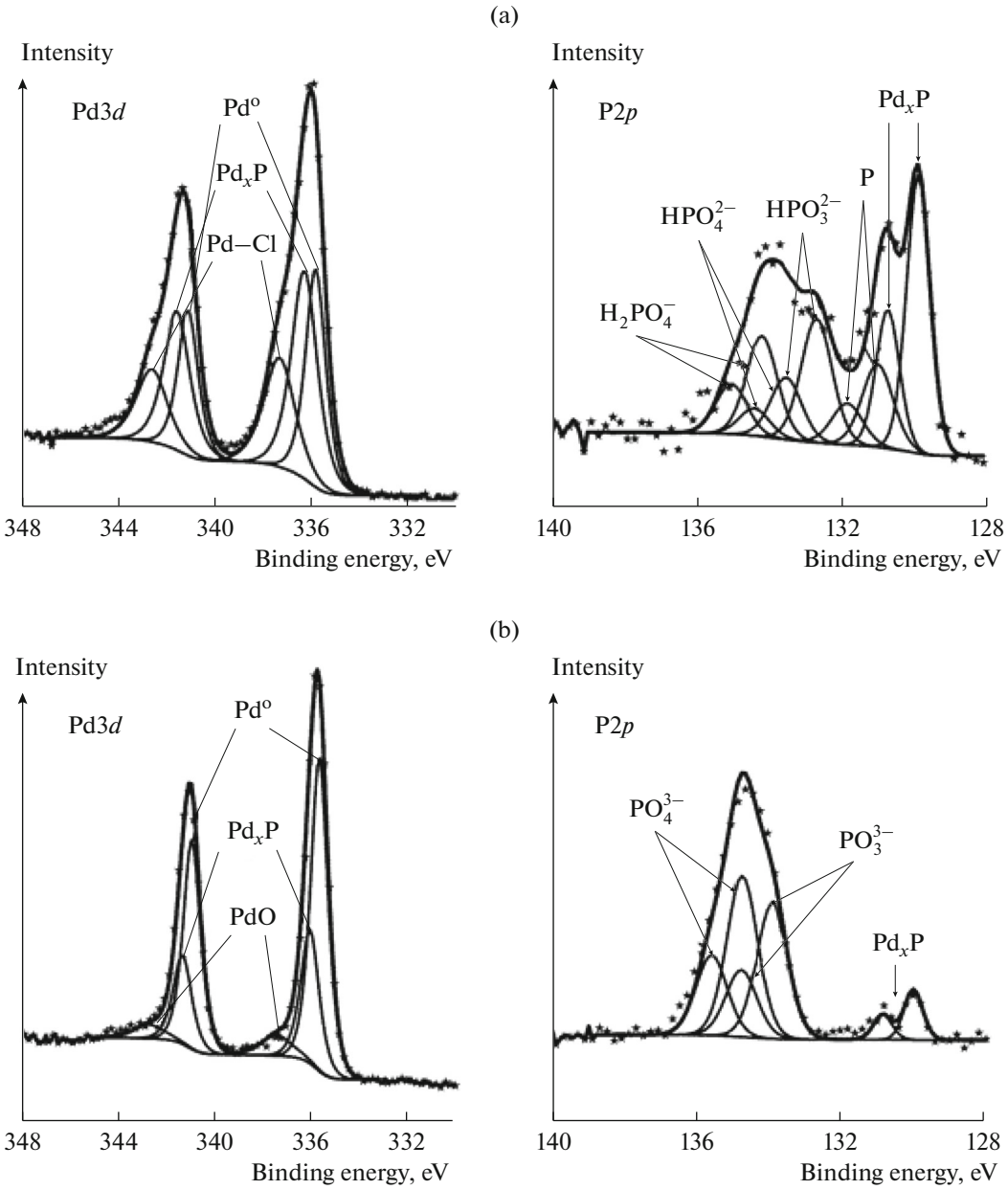

Fig. 3. Pd3*d* and P2*p*, photoelectron spectra recorded before the ion sputtering of (a) sample 1 ($PdCl_2$–0.3P) and (b) sample 2 ($Pd(acac)_2$–0.7P).

via a metal particle formation stage followed by phosphorus migration into the metal nanocluster and subsequent metal phosphide crystallization [22]. We think that the possibility of the low-temperature synthesis of the palladium phosphides is due to the palladium precursor being a palladium compound in the molecular dispersed state and palladium atoms forming from this compound. The fact that the reactivity of the palladium clusters toward white phosphorus is low compared to the reactivity of the Pd(0) atoms and the mild catalyst formation conditions (30°C, $P_{H_2} = 2$ atm) are the reasons why the surface of the Pd–P catalyst is enriched with phosphorus at P/Pd = 0.3.

Note that a similar qualitative composition of the surface layer is observed for the Pd–P catalyst formed from $Pd(acac)_2$ and white phosphorus in a hydrogen atmosphere (P/Pd = 0.7, sample 2, Fig. 3). As was mentioned above, both catalysts show similar properties in *o*-CNB hydrogenation. In the surface layer of sample 2, palladium is mainly in two chemical forms, namely, small clusters (BE(Pd3$d_{5/2}$) = 335.6 eV) and a phosphide (BE(Pd3$d_{5/2}$) = 336.0 eV, BE(P2$p_{3/2}$) =

Table 4. Binding energies and concentrations of elements in different states in the surface layer of the Pd–P catalyst prepared from $Pd(acac)_2$ and P_4 in a hydrogen atmosphere (P/Pd = 0.7)

Spectral line	Binding energy, eV	FWHM, eV	Element concentration, at %	Most likely chemical species*
Before sputtering				
Pd3$d_{5/2}$	335.6	0.8	8.2	Pd^0 (0.63)
	336.0	0.9		Pd_xP (0.29)
	337.4	1.5		PdO (0.08)
P2$p_{3/2}$	130.0	0.6	22.0	Pd_xP (0.09)
	133.9	1.0		PO_3^{3-} (0.41)
	134.7	1.0		PO_4^{3-} (0.50)
N1s	402.1	1.4	3.4	$[NH_2R_2]^+$ (1.0)
O1s	531.5	1.5	20.6	PO_3^{3-}, PO_4^{3-} (1.0)
C1s	284.2	0.8	45.8	Pd–C, graphite (0.15)
	284.9	1.3		C–H, C–C (0.48)
	286.3	1.5		$[NH_2R_2]_2X$ (C–N) (0.29)
	288.9	1.4		acacH (C=O) (0.08)
After 1-min-long sputtering				
Pd3$d_{5/2}$	335.6	0.7	22	Pd^0 (0.32)
	336.0	1.0		Pd_xP (0.62)
	337.7	1.5		PdO (0.06)
P2$p_{3/2}$	130.1	0.7	78	Pd_xP (0.07)
	133.8	1.0		PO_3^{3-} (0.28)
	134.6	1.0		PO_4^{3-} (0.65)

* The number in parentheses is the atomic fraction of the species.

130.0 eV) in a ratio of 2.17 : 1 (Table 4). The empirical formula of the surface phosphide is $Pd_{1.2}P$. The subsurface layer of the P/Pd = 0.7 catalyst (after 1-min-long sputtering) has the same qualitative composition as the surface layer but differs from the latter in the proportions of chemical forms of Pd and P. In the surface layer of sample 2, palladium clusters are 2 times less abundant than palladium phosphides (Pd(0) : Pd_xP = 1 : 1.94). The composition of palladium phosphides in the subsurface layer can be represented by the empirical formula Pd_5P_2. If it is neglected that the phase composition of the nanoparticles may vary with depth, it can be concluded that the dominant palladium phosphide in sample 2 is Pd_5P_2. Accordingly, it can be supposed that the empirical formula of the surface phosphide—$Pd_{1.2}P$—characterizes a mixture of Pd_5P_2 and PdP_2 in a ratio of 0.35 : 0.65. The inference that sample 2 is dominated by Pd_5P_2 is consistent with HRTEM data. The high-resolution images indicate interplanar spacings of 2.18 and 2.29 Å (Fig. 4), which pertain to Pd_5P_2 (d/n = 2.183 and 2.288 Å; # 00-019-0887). The micrographs of the $Pd(acac)_2$–0.7P system, as distinct from those of the system involving palladium dichloride, indicate the presence of not only 3–5 nm particles but also larger particles ~20 nm in diameter (Fig. 4a), which are polycrystallites, according to STEM images obtained in the Z-contrast mode (Fig. 4b) and FFT mode (Fig. 4f).

Thus, modification with phosphorus increases the degree of dispersion of the palladium catalyst and favors the formation, under mild conditions, of particles containing different palladium phosphides and palladium clusters. In recent years, transition metal phosphides have been considered as a new class of catalysts for hydrotreating processes, namely, hydrodesulfurization and hydrodenitrogenation [15, 20]. It would, therefore, be expected that both palladium phosphide and palladium clusters will be catalytically active in hydrogenation processes. More resistant to deactivation, transition metal phosphides exhibit their catalytic activity under fairly severe conditions, specif-

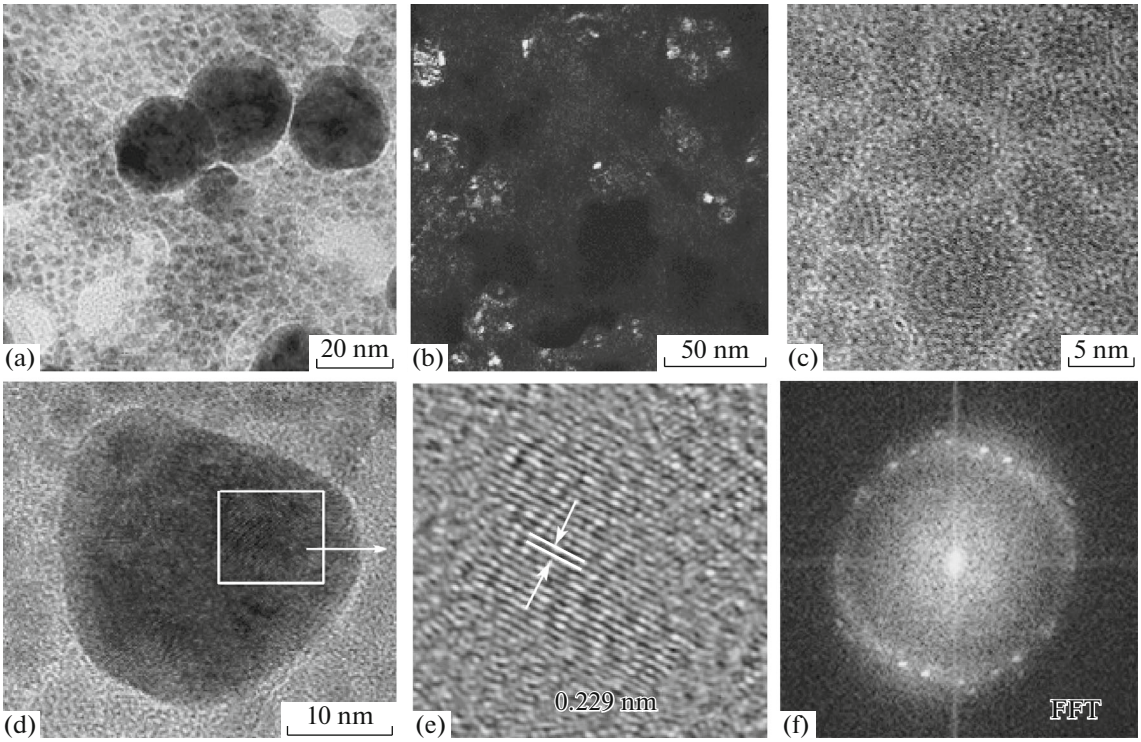

Fig. 4. (a, c) TEM images of the $Pd(acac)_2$–0.7P–H_2 system formed in DMF ($C_{Pd(acac)2}$ = 5 mmol/L); (b) STEM (Z-contrast) image; (d, e) HRTEM images; (f) FFT pattern.

ically at temperatures of 250–300°C and a hydrogen pressure of 30 atm [22]. However, in alkene and diene hydrogenation reactions, transition metal phosphides are much less active than metal catalysts [11]. Moreover, using the $Pd(dba)_2$ complex and white phosphorus as a catalyst in styrene hydrogenation under mild conditions as an example, we demonstrated earlier that the activity of the catalyst is inversely proportional to the P/Pd ratio in the 0–1.2 range, indicating that the introduction of P_4 converts part of the palladium into a species that is inactive under mild conditions [47]. In addition, the formation of different palladium phosphides along with palladium clusters was proved. Therefore, the main contribution to the hydrogenation catalysis under mild conditions is made by the palladium clusters. A common feature of samples 1 and 2, which show similar properties in *o*-CNB hydrogenation, is that they contain small palladium clusters. It is, therefore, logical to attribute the increased *o*-CNB hydrogenation selectivity of these samples to the formation of the small palladium clusters.

CONCLUSIONS

An analysis of the experimental data presented here and our earlier data [26] elucidated the major factors having an effect on the nature and, accordingly, activity and chemoselectivity of phosphorus-modified palladium catalysts in *o*-CNB hydrogenation. The synthesis of palladium catalysts using elemental phosphorus in a hydrogen atmosphere yields Pd–P nanoparticles whose phase composition, surface state, and size depend on the P/Pd ratio, nature of the acido ligand in the precursor, and precursor concentration. At P/Pd = 0.3 ($Pd(acac)_2$ precursor), the synthesis of the catalyst yields palladium-enriched polycrystalline particles, their core consisting of palladium phosphides ($Pd_3P_{0.8}$, Pd_6P) and their shell made up by Pd nanoclusters [48].With an increasing P/Pd ratio, the proportion of palladium clusters decreases (because an increasing part of the Pd(0) atoms turns into phosphides), the size of the Pd(0) clusters decreases, and the phase composition of the resulting palladium phosphides changes in the following order: $Pd_3P_{0.8} \rightarrow Pd_5P_2 \rightarrow PdP_2$. Therefore, depending on the P/Pd ratio and acido ligand nature in the precursor, the promoting effect of phosphorus and on the chemoselectivity of the palladium catalysts in *o*-CNB hydrogenation can be due to two factors hampering the hydrogenolysis of the C–Cl bond. The first factor is a thermodynamic one: the ratio of the adsorption equilibrium constant of *o*-CNB to that of *o*-CA increases because the binding energy of the *d* electrons of Pd(0) nanoclusters in the palladium-enriched Pd–P nanoparticles (BE($Pd3d_{5/2}$) = 334.5 eV) is lower than the same binding energy for the bulk metal ($Pd(acac)_2$ precursor, P/Pd = 0.3) [26]. The second factor is the formation of "electron-deficient" small palladium

clusters (BE(Pd3$d_{5/2}$) = 335.7 eV) responsible for *o*-CNB hydrogenation under mild conditions (P/Pd = 0.7 for the $Pd(acac)_2$ precursor, and P/Pd = 0.3 for the $PdCl_2$ precursor). An increase in selectivity in *o*-CNB hydrogenation was also observed for a Pt/γ-Fe_2O_3 catalyst containing "electron-deficient" platinum clusters [49]. Elucidation of the causes of the higher selectivity of "electron-deficient" metal clusters in the hydrogenation of nitrohaloarenes needs further theoretical studies. On the one hand, these clusters must form stronger bonds with nucleophilic molecules (haloanilines). If this is the case, then, if only the thermodynamic factor were taken into account, the selectivity would decrease, not increase. However, electron donor groups (e.g., the amino group) are known to activate the C–Hal bond, shifting electron density to the halogen atom and thereby facilitating the hydrogenolysis of this bond [50]. It is due to this circumstance that haloanilines rather than nitrohaloarenes mainly undergo hydrogenolysis. Therefore, it is logical to suppose that it is the low capacity of the "electron-deficient" clusters to reverse bonding with the aromatic ring of the haloaniline that hampers the hydrogenolysis of the C–Hal bond. On the other hand, the following geometric factor cannot be disregarded: the planar adsorption of *o*-CA molecules on small clusters is sterically difficult.

Along with the two above-considered ways of enhancing the selectivity of the Pd–P catalysts, there is a third way, which is based on optimizing the reaction conditions, including selection of a solvent—a factor having a significant effect on the yield of condensation products (azo and azoxy derivatives) [9].

Thus, the ratio between the variously sized palladium clusters and the palladium phosphides (which function as a support in the case of $Pd(acac)_2$ used as the precursor under mild conditions), depending on the Pd–P catalyst formation conditions (nature of the acido ligand in the precursor and P/Pd ratio) is the main factor in the modifying action of phosphorus on the palladium catalysts for hydrogenation.

ACKNOWLEDGMENTS

This study was carried out in the framework of the project part of state assignment no. 4.353.2014/K from the Ministry of Education and Science of the Russian Federation. The electron micrographs of the catalysts were obtained on an electron microscope at the Baikal Nanotechnology Center shared facilities of Irkutsk National Research Technical University. The authors are grateful to Yu.L. Mikhlin (Institute of Chemistry and Chemical Technology, Siberian Branch, Russian Academy of Sciences, Krasnoyarsk) for recording X-ray photoelectron spectra.

REFERENCES

1. Coq, B. and Figueras, F., *Coord. Chem. Rev.,* 1998, vols. 178–180, p. 1753.
2. Wang, X., Liang, M., Zhang, J., and Wang, Y., *Curr. Org. Chem.,* 2007, vol. 11, p. 299.
3. Blaser, H.U., *Science,* 2006, vol. 313, p. 312.
4. Krátky, V., Králik, M., Kaszonyi, A., Štolcová, M., Zalibera, L., Mečárová, M., and Hronec, M., *Collect. Czech. Chem. Commun.,* 2003, vol. 68, p. 1819.
5. Meng, X., Cheng, H., Fujita, S., Hao, Y., Shang, Y., Yu, Y., Cai, S., Zhao, F., and Arai, M., *J. Catal.,* 2010, vol. 269, p. 131.
6. Ichikawa, S., Seki, T., and Ikariya, T., *Adv. Synth. Catal.,* 2014, vol. 356, p. 1.
7. Cheng, H., Meng, X., He, L., Lin, W., and Zhao, F., *J. Colloid Interface Sci.,* 2014, vol. 415, p. 1.
8. Skripov, N.I., Belykh, L.B., Sterenchuk, T.P., and Schmidt, F.K., *Russ. J. Appl. Chem.,* 2015, vol. 88, no. 8, p. 1255.
9. Corma, A., Serna, P., Concepción, P., and Calvino, J.J., *J. Am. Chem. Soc.,* 2008, vol. 130, p. 8748.
10. Baumeister, P., Blaser, P.U., Siegrist, U., and Studer, M., *Catal. Org. React.,* 1998, vol. 75, p. 207.
11. Mitsudome, T. and Kaneda, K., *Green Chem.,* 2013, vol. 15, p. 2636.
12. Cárdenas-Lizana, F., Pedro, Z.M., Gómez-Quero, S., and Keane, M.A., *J. Mol. Catal. A: Chem.,* 2010, vol. 326, p. 48.
13. Boronat, M., Concepción, P., Corma, A., González, S., Illas, S., and Serna, P., *J. Am. Chem. Soc.,* 2007, vol. 129, p. 16230.
14. Campos, C.H., Jofre, M., Torres, C., Pawelec, B., Fierro, J.L.G., and Reyes, P., *Appl. Catal., A,* 2014, vol. 482, p. 127.
15. Bowker, R.H., Smith, M.C., Carrillo, B.A., and Bussell, M.E., *Top. Catal.,* 2012, vol. 55, nos. 14–15, p. 999.
16. Kanda, Y., Temma, Y., Nakata, K., Kobayashi, T., Sugioka, M., and Uemichi, Y., *Appl. Catal., A,* 2010, vol. 386, no. 1, p. 171.
17. Savithra, G.H.L., Bowker, R.H., Carrillo, B.A., Bussell, M.E., and Brock, S.L., *ACS Appl. Mater. Int.,* 2013, vol. 5, no. 12, p. 5403.
18. Sweeney, C.M., Stamm, K.L., and Brock, S.L., *J. Alloys Compd.,* 2008, vol. 448, no. 1, p. 122.
19. Oyama, S.T., Gott, T., Zhao, H., and Lee, Y-K., *Catal. Today,* 2009, vol. 143, p. 94.
20. Bui, P., Cecilia, J.A., Oyama, S.T., Takagaki, A., Infantes-Molina, A., Zhao, H., Li, D., Rodríguez-Castellón, E., and Jiménez-Lopéz, A., *J. Catal.,* 2012, vol. 294, p. 184.
21. Muetterties, E.L. and Sauer, J.C., *J. Am. Chem. Soc.,* 1974, vol. 96, no. 11, p. 3410.
22. Prins, R. and Bussell, M.E., *Catal. Lett.,* 2012, vol. 142, no. 12, p. 1413.
23. Cecilia, J.A., Jimenéz-Moralesa, I., Infantes-Molina, A., and Rodríguez-Castellón, E., *J. Mol. Catal. A: Chem.,* 2013, vol. 368-369, p. 78.
24. Belykh, L.B., Skripov, N.I., Belonogova, L.N., Umanets, V.A., and Shmidt, F.K., *Kinet. Catal.,* 2010, vol. 51, no. 1, p. 42.

25. Skripov, N.I., Belykh, L.B., Belonogova, L.N., Umanets, V.A., Ryzhkovich, E.N., and Schmidt, F.K., *Kinet. Catal.,* 2010, vol. 51, no. 5, p. 714.
26. Belykh, L.B., Skripov, N.I., Stepanova, T.P., and Schmidt, F.K., *Kinet. Catal.,* 2015, vol. 56, no. 2, p. 181.
27. Gordon, A.J. and Ford, R.A., *The Chemist's Companion,* New York: Wiley, 1972.
28. US Patent 3474464. http://www.google.com.tr/patents/US3474464.
29. *Preparatyka organiczna,* Polaczkova, W., Ed., Warsaw: Państwowe Wydawnistwa Techniczne, 1954.
30. Ukai, T., Kawazura, H., Ishii, Y., Bonnet, J.J., and Ibers, J.A., *J. Organomet. Chem.,* 1974, vol. 65, p. 253.
31. Moreno-Maiias, M., Pajuelo, F., and Pleixats, R., *J. Org. Chem.,* 1995, vol. 60, no. 8, p. 2396.
32. Ma, L., Chen, S., Lu, C., Zhang, Q., and Li, X., *Catal. Today,* 2011, vol. 173, p. 62.
33. http://link.springer.com/article/10.1007/BF02667684.
34. *Successful Design of Catalysts,* Inui, T., Ed., Amsterdam: Elsevier, 1988, p. 3.
35. Grosvenor, A.P., Cavell, R.G., and Mar, A., *Struct. Bond.,* 2009, vol. 133, p. 41.
36. Gabasch, H., Unterberger, W., Hayek, K., Klötzer, B., Kleimenov, E., Teschner, D., Zafeiratos, S., Hävecker, M., Knop-Gericke, A., Schlögl, R., Han, J., Ribeiro, F.H., Aszalos-Kiss, B., Curtin, T., and Zemlyanov, D., *Surf. Sci.,* 2006, vol. 600, p. 2980.
37. Wertheim, G.K., *Z. Phys. D: At. Mol. Clusters,* 1989, vol. 12, nos. 1–4, p. 319.
38. Mason, M.G., *Phys. Rev. B: Condens. Matter,* 1983, vol. 27, no. 2, p. 748.
39. Wu, T., Kaden, W.E., Kunkel, W.A., and Anderson, S.L., *Surf. Sci.,* 2009, vol. 603, p. 2764.
40. Hara, M., Asami, K., Hashimoto, K., and Masumoto, T., *Electrochim. Acta,* 1983, vol. 28, no. 8, p. 1073.
41. Hara, M., Asami, K., Hashimoto, K., and Masumoto, T., *Electrochim. Acta,* 1986, vol. 31, no. 4, p. 481.
42. Gniewek, A., Trzeciak, A.M., Ziólkowski, J.J., Kepiński, L., Wrzyszcz, J., and Tylus, W., *J. Catal.,* 2005, vol. 229, p. 332.
43. Hasik, M., Bernasik, A., Drelinkiewicz, A., Kowalski, K., Wenda, E., and Camra, J., *Surf. Sci.,* 2002, vol. 507, p. 916.
44. Swift, P., *Surf. Interface Anal.,* 1982, vol. 4, no. 2, p. 47.
45. Sun, H., Xu, J., Fu, G., Mao, X., Zhang, L., Chen, Y., Zhou, Y., Lu, T., and Tang, Y., *Electrochim. Acta,* 2012, vol. 59, p. 279.
46. Carenco, S., Hu, Y., Florea, I., Ersen, O., Boissiere, C., Sanchez, C., and Mezailles, N., *Dalton Trans.,* 2013, vol. 42, p. 12667.
47. Belykh, L.B., Skripov, N.I., Belonogova, L.N., Umanets, V.A., Stepanova, T.P., and Schmidt, F.K., *Kinet. Catal.*, 2011, vol. 52, no. 5, p. 702.
48. Belykh, L.B., Skripov, N.I., Stepanova, T.P., Akimov, V.V., Tauson, V.L., and Schmidt, F.K., *Curr. Nanosci.,* 2015, vol. 11, no. 2, p. 175.
49. Zhang, J., Wang, Y., Ji, H., Wei, Y., Wu, N., Zuo, B., and Wang, Q., *J. Catal.,* 2005, vol. 229, p. 114.
50. Pietrowski, M., *Curr. Org. Synth.,* 2012, vol. 9, p. 470.

Translated by D. Zvukov